

Electronic States at Edges of Finite p -orbital Helical Atomic Chain

Takemitsu Kato,¹ Yasuhiro Utsumi,¹ Ora Entin-Wohlman,² and Amnon Aharony²

¹*Department of Physics Engineering, Faculty of Engineering, Mie University*

²*School of Physics and Astronomy, Tel Aviv University*

(Dated: 31 May 2023)

In connection to the chirality induced spin-selectivity (CISS) effect, we theoretically analyze the electron state of edges of a finite p -orbital helical atomic chain with the intra-atomic spin orbit interaction (SOI). This model can host the spin-filtering state in which two up spins propagate in one direction and two down spins propagate in the opposite direction without breaking the time-reversal symmetry. We found that this model can exhibit the enhancement of charge density concentrated at the edges due to the evanescent states induced by the spin and orbital flip by the SOI. Although the spin density is absent because of the time reversal symmetry of the SOI, the charge concentration at the edges may play a role in the enantioselective adsorption of CISS molecules on the ferromagnetic surface.

I. INTRODUCTION

The chiral-induced spin selectivity (CISS) effect is a spin transport phenomenon that is specific to chiral materials: When an electron is injected into chiral molecules such as DNA, the electron spin is selectively separated depending on the chirality. This phenomenon exhibits a high spin polarization rate compared to ordinary magnetic materials, and has attracted attention as a quantum phenomenon that occurs at room temperature.¹ Although the CISS effect has been observed in many experiments using various chiral materials, a fully convincing theoretical explanation has not yet been proposed.²

There is another interesting phenomenon associated to the CISS, the enantioselectivity: Molecules with a specific chirality selectively adsorbed to the surface of the magnetic substrate.³⁻⁵ Theoretically this effect is explained as the consequence of the spin-dependent dispersion force,^{4,6} the charge redistribution of the molecule attached to substrate.⁷ Reference 8 argued that the electric toroidal monopole is behind this phenomenon. Another experimental paper suggested that the chiral molecule attached to the superconducting substrate induces the Shiba state.⁹

In the above mentioned works, the spin and electric state at the edge of the chiral molecule seem to be important. In this study, we analyze this issue using a p -orbital helical atomic chain with the intra-atomic spin-orbit interaction (SOI), which is a toy model of helical molecules such as DNA.^{10,11} Previously, we calculated the band structure of an infinite chain¹⁰ and the transmission probability of the molecular junction¹¹ to investigate the spin filtering. In this paper, we focused on the finite molecular chain to analyze the behavior of spin at the ends. In the presence of the strong crystal field along the tangential direction of the helix, this model is effectively reduced to the two-orbital channel one dimensional chain with the SOI, which flips both the spin and orbital channels, see Fig. 1. More explicitly, the effective Hamiltonian may be written as follows:

$$V = a c_{p_z; k \uparrow}^\dagger c_{p_x; -k \downarrow} - a c_{p_x; k \uparrow}^\dagger c_{p_z; -k \downarrow} + a^* c_{p_x; -k \downarrow}^\dagger c_{p_z; k \uparrow} - a^* c_{p_z; -k \downarrow}^\dagger c_{p_x; k \uparrow}, \quad (1)$$

where a is a complex number. Here $c_{o; k \sigma}$ is an annihilation operator of an electron with the orbital channel o ($= p_x, p_z$),

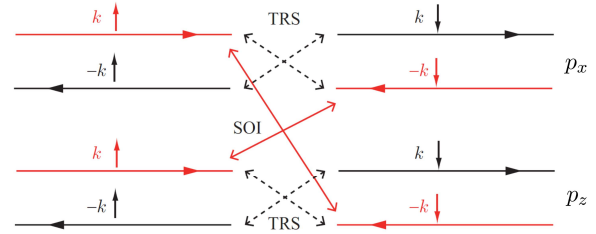


FIG. 1. Schematic picture of the two-terminal and two-orbital spin filtering mechanism. Different orbitals are mixed by the SOI, allowing the creation of opposite-spin states that flow in the opposite direction while maintaining time-reversal symmetry.

the wave number k and the spin σ ($= \uparrow, \downarrow$). This Hamiltonian is even under the time reversal, $\hat{\Theta} V \hat{\Theta}^{-1} = V$, where $\hat{\Theta}$ is the time reversal operator.

The Hamiltonian Eq. (1) hybridizes the right going \uparrow -spins and the left-going \downarrow -spins and forms a standing wave. As a consequence the left-going \uparrow -spins and the right-going \downarrow -spins form the helical state, which is responsible for the spin-filtering. One can naively expect that, in a finite chain, the \downarrow -spin accumulates at one edge and the \uparrow -spin accumulates at the other edge. We will discuss this issue in this paper.

The structure of the paper is the following: In Sec. II, we introduce the p -orbital helical atomic chain and present out numerical results. Furthermore, we present an analytic explanation of the electron state at the edges in Sec. III. Section IV concludes our findings.

II. p -ORBITAL HELICAL ATOMIC CHAIN

The position of an atom on the helical atomic chain [Fig. 2] is,

$$\mathbf{R}(\phi_n) = [R \cos(\phi_n), R \sin(\phi_n), \Delta h \phi_n / (2\pi)]. \quad (2)$$

where R , n , Δh and $\phi_n = \Delta \phi \cdot n$ represent the radius, site number, the pitch, and the rotation angle around the z -axis. Here

$p=+1(-1)$ indicates the left(right)-handed helix. The angle between the neighbouring atoms is set $\Delta\phi = 2\pi/N$, where N is the number of atoms in a unit cell. The helix is characterized by the torsion τ and the curvature $\kappa = \sqrt{1 - \tau^2}$:

$$\tau = \frac{p\Delta h/(2\pi)}{\sqrt{R^2 + [\Delta h/(2\pi)]^2}}. \quad (3)$$

The Hamiltonian of the helical atomic chain [Fig. 2] is given by,

$$H = \sum_{n=1}^{MN} \left(-\tilde{c}_{n+1}^\dagger \mathbf{J} \otimes \sigma_0 \tilde{c}_n + \text{H.c.} \right. \\ \left. + \Delta_{\text{so}} \tilde{c}_n^\dagger \mathbf{L} \cdot \boldsymbol{\sigma} \tilde{c}_n \right. \\ \left. + K_t \tilde{c}_n^\dagger \left[(\mathbf{t}(\phi_n) \cdot \mathbf{L})^2 - 1_3 \right] \otimes \sigma_0 \tilde{c}_n \right), \quad (4)$$

where M is the number of unit cells and σ_i ($i = x, y, z$) represents the Pauli matrix and σ_0 represents a 2×2 unit matrix in spin space. The n -th atom hosts two p orbitals and the vector of creation operators is

$$\tilde{c}_n^\dagger = [\tilde{c}_{n;x\uparrow}^\dagger \ \tilde{c}_{n;x\downarrow}^\dagger \ \tilde{c}_{n;y\uparrow}^\dagger \ \tilde{c}_{n;y\downarrow}^\dagger \ \tilde{c}_{n;z\uparrow}^\dagger \ \tilde{c}_{n;z\downarrow}^\dagger], \quad (5)$$

where $c_{n;x(y)\sigma}^\dagger$ creates σ spin at the $p_x(p_y)$ orbitals of an atom at site n . The first line of this Hamiltonian represents the hopping of electrons between nearest-neighbor sites. The system satisfies the helical symmetry and the matrix \mathbf{J} is parameterized by 3 real numbers J , α , and φ ,¹⁰

$$\mathbf{J} = J \begin{pmatrix} \alpha \cos \varphi & \alpha \sin \varphi & 0 \\ -\alpha \sin \varphi & \alpha \cos \varphi & 0 \\ 0 & 0 & 1 \end{pmatrix}. \quad (6)$$

In the following, we take $J > 0$. The second line is for the atomic spin-orbit interaction, where $\boldsymbol{\sigma}$ is the vector of Pauli matrices and $\mathbf{L} = (L_x, L_y, L_z)$ is the vector of the orbital angular momentum operators:

$$L_x = \begin{pmatrix} 0 & 0 & 0 \\ 0 & 0 & -i \\ 0 & i & 0 \end{pmatrix} \quad (7)$$

$$L_y = \begin{pmatrix} 0 & 0 & i \\ 0 & 0 & 0 \\ -i & 0 & 0 \end{pmatrix} \quad (8)$$

$$L_z = \begin{pmatrix} 0 & -i & 0 \\ i & 0 & 0 \\ 0 & 0 & 0 \end{pmatrix} \quad (9)$$

The third line describes the crystalline field with the amplitude K_t in the tangent direction,

$$\mathbf{t}(\phi_n) = [-\kappa \sin(\phi_n), p\kappa \cos(\phi_n), |\tau|]. \quad (10)$$

Figures 3 (a-1,2) show the band structures of the infinite chain for various parameters. In each panel, we observe two

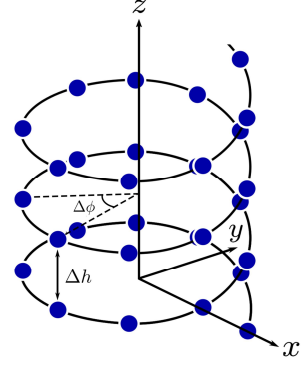


FIG. 2. Schematic picture of a helical atomic chain. The model is a right-handed system in which the z -axis coincides with the helical axis.

bands separated by K_t . The panel (a-1) corresponds to the ideal spin-filtering condition^{10,11}, see Eq. (13). The helical states corresponding to Fig. 1 are formed in the avoided crossing, the center of which is indicated by the horizontal dashed line at $E_F = -2J \cos \frac{\pi}{N}$. The panel (a-2) is the band structure with parameters away from the ideal spin-filtering condition. We still observe the two helical states around the horizontal dashed line.

Figures 3 (b-1,2) show the local charge density for a finite chain with parameters corresponding to the panels (a-1,2). The local charge density is defined as,

$$\langle \rho \rangle_n = \sum_{E < E_F} \langle E | \rho_n | E \rangle, \quad (11)$$

$$\rho_n = \Pi_n \otimes I_3 \otimes \sigma_0, \quad (12)$$

where the projection operator is a $MN \times MN$ matrix $(\Pi_n)_{i,j} = \delta_{i,n} \delta_{j,n}$ and $H|E\rangle = E|E\rangle$. The Fermi level is taken at the center of the avoided crossing at $E_F = -2J \cos \frac{\pi}{N}$, see the horizontal dashed lines in panels (a-1,2). In each panel, the solid line and the dashed line are results with and without SOI. We observe the oscillations of charge density in the absence of the SOI. When the SOI is present, the oscillations in the bulk region are suppressed and the modulations are concentrated at the edges of the molecule.

In a single orbital, two electrons can be accommodated, leading to the complete occupancy of the lower p_y orbital. The upper band, formed by the mixing of the p_x and p_z orbitals, positions the Fermi level at approximately one-fourth of the band width in the panels (a-1,2). Consequently, the average occupancy of electrons is one. This can be regarded as the reason for the fluctuation of the charge density around three in the panels (b-1,2).

In the next section, we analyze this charge concentration.

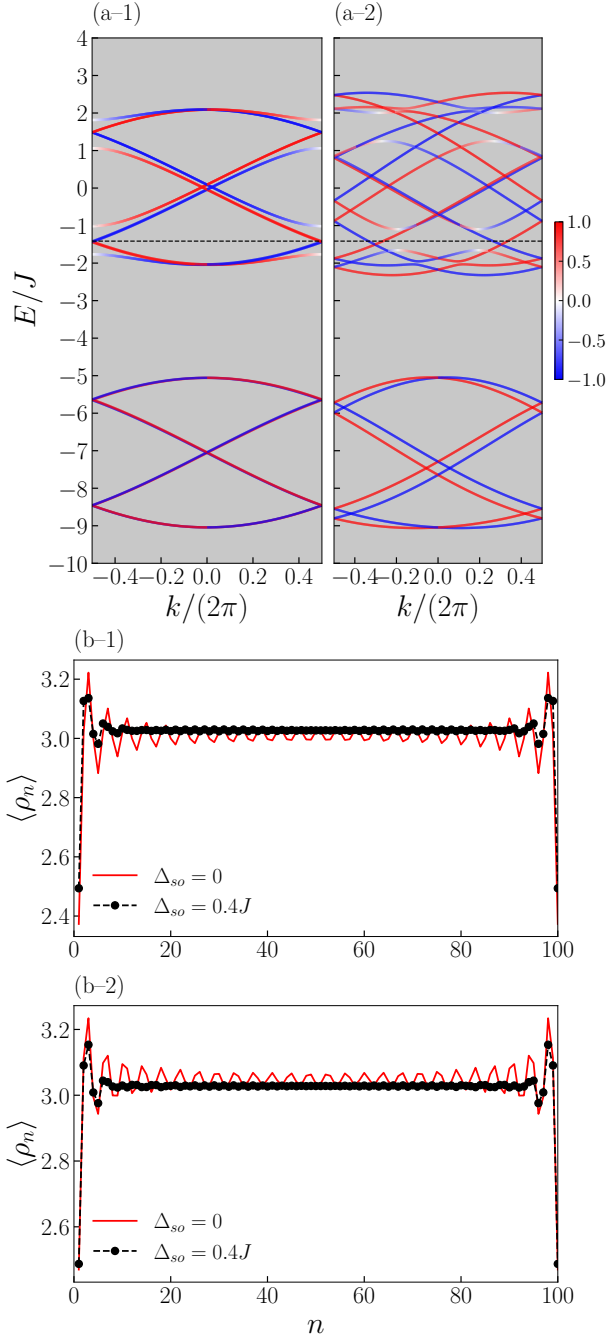


FIG. 3. (a-1,2) Band structures for various parameters: $\alpha = 1$, $\varphi = \Delta\phi$ and $\tau = 0$ for (a-1) and $\alpha = \sqrt{2}$, $\varphi = \Delta\phi/2$ and $\tau = 0.48$ for (a-2). Other parameters are fixed as $p = 1$ and $K_t = 7J$. The colors represent the expectation value of the z -component of spin. (See the color bar.) (b-1,2) Integrated charge densities of electrons occupying up to the Fermi level $E_F = -2J \cos \frac{\pi}{N}$ for a finite chain $M = 25$ and $N = 4$. Parameters of the panels (b-1,2) correspond to those of the panels (a-1,2). In each panel of (a-1,2), the Fermi level is indicated by the dashed line. The marked black dashed line and red solid line indicate the local charge density with SOI $\Delta_{so} = 0.4J$ and without it $\Delta_{so} = 0$.

III. ANALYTIC RESULTS FOR THE LOCAL CHARGE DENSITY

In this section, we derive an analytic expression of the local charge density. To make our analysis simpler, we focus on the following conditions: The torsion is zero, $\tau = 0$, the crystalline field along the tangential direction is infinite $K_t \rightarrow -\infty$, $\alpha = 1$ and $\varphi = -p\Delta\phi$ in Eq. (6). Then the original Hamiltonian, Eq. (4) can be split into time-reversal symmetric pairs, $H = H_+ + H_-$, where H_{\pm} are represented as

$$H_{\pm} = \sum_{n=1}^{MN} \left(-Jc_{n+1;\pm}^{\dagger}c_{n;\pm} + \text{H.c.} \right. \\ \left. \pm p\Delta_{so}c_{n;\pm}^{\dagger} \begin{bmatrix} 0 & e^{-ip\phi_n} \\ e^{ip\phi_n} & 0 \end{bmatrix} c_{n;\pm} \right). \quad (13)$$

In this coordinate system, we use the rotation operator $O_n = e^{iL_z p\phi_n}$ of site n to perform a local coordinate transformation on \mathbf{J} , $c_n = O_n \tilde{c}_n$. The creation operators can be written as a pseudospin space:

$$c_{n;+}^{\dagger} = [c_{n;x\uparrow}^{\dagger} \ c_{n;z\downarrow}^{\dagger}], \quad (14)$$

$$c_{n;-}^{\dagger} = [c_{n;x\uparrow}^{\dagger} \ c_{n;x\downarrow}^{\dagger}]. \quad (15)$$

H_+ hybridizes the up-spin in the p_x orbital and the down-spin in the p_z orbital, and H_- hybridizes the down-spin in the p_x orbital and the up-spin in the p_z orbital.

In the following, we consider H_+ . In order to diagonalize Eq. (13), we take the scattering theory approach¹². In this case, we first consider an infinite chain \hat{H}_+ and impose a boundary condition. The eigenenergies of \hat{H}_+ are

$$E_{\pm} = E_S(z_{k,p}) \pm p\sqrt{E_A(z_{k,p})^2 + \Delta_{so}^2}, \quad (16)$$

where,

$$z_{k,p} = e^{i\frac{k+2\pi p}{N}}, \quad (17)$$

$$E_{S/A}(z_{k,p}) = \frac{E(z_{k,p}) \pm E(z_{k,p}e^{i\Delta\phi})}{2}, \quad (18)$$

$$E(z_{k,p}) = -J(z_{k,p} + z_{k,p}^{-1}). \quad (19)$$

Figure 4(a) shows the energy eigenvalue as a function of k . The upper (lower) branch corresponds to $E_+(E_-)$. If the SOI is absent, the two branches intersect at $E_{0,\pm} = \pm 2J \cos \frac{\pi}{N}$. The corresponding eigen ket is,

$$|z_{k,p}; \pm\rangle = \sum_{n=-\infty}^{\infty} z_{k,p}^n \hat{c}_{n;\pm}^{\dagger}(z_{k,p}) |0\rangle, \quad (20)$$

$$\hat{c}_{n;-}^{\dagger}(z_{k,p}) = u(z_{k,p})c_{n;x\uparrow}^{\dagger} - v(z_{k,p})e^{ip\phi_n}c_{n;z\downarrow}^{\dagger}, \quad (21)$$

$$\hat{c}_{n;+}^{\dagger}(z_{k,p}) = v(z_{k,p})c_{n;x\uparrow}^{\dagger} + u(z_{k,p})e^{ip\phi_n}c_{n;z\downarrow}^{\dagger}, \quad (22)$$

where,

$$u(z_{k,p}) = \sqrt{\frac{1}{2} \left(1 - \frac{pE_A(z_{k,p})}{\sqrt{E_A(z_{k,p})^2 + \Delta_{\text{so}}^2}} \right)}, \quad (23)$$

$$v(z_{k,p}) = \sqrt{\frac{1}{2} \left(1 + \frac{pE_A(z_{k,p})}{\sqrt{E_A(z_{k,p})^2 + \Delta_{\text{so}}^2}} \right)}. \quad (24)$$

In the following, we focus on the right-handed coordinate system, $p = 1$. We first find the four values of $z_{k,p}$, which are the solutions of $E = E_{\pm}$, see Eq. (16):

$$z_{s,s'} = e^{-i\frac{\Delta\phi}{2}} \left(\xi_s - s' \sqrt{\xi_s^2 - 1} \right), \quad (25)$$

$$\xi_s = -\frac{E}{2J} \cos \frac{\pi}{N} + s \sqrt{\left[1 - \left(\frac{E}{2J} \right)^2 \right] \sin^2 \frac{\pi}{N} + \left(\frac{\Delta_{\text{so}}}{2J} \right)^2}, \quad (26)$$

where $s, s' = \pm$. The eigen ket associated with a given energy E is then a linear combination of Eq. (20) with these four values of $z_{k,p}$,

$$|E\rangle = \sum_{s,s'=\pm} a_{s,s'} |z_{s,s'}; \sigma_s\rangle, \quad (27)$$

where $\sigma_s = +$ or $-$. The probability amplitude at site n is then

$$\psi(n) = \begin{pmatrix} \psi_{\uparrow}(n) \\ \psi_{\downarrow}(n) \end{pmatrix} = \begin{pmatrix} \langle n; \uparrow | E \rangle \\ \langle n; \downarrow | E \rangle \end{pmatrix}. \quad (28)$$

where we write $|n; \sigma\rangle = c_{n;o\sigma}^{\dagger} |0\rangle$ ($o = x, z$).

The 4 coefficients $a_{s,s'}$ and the energy E are determined to satisfy the boundary condition consisting of 4 equations (see Appendix B) and the normalization condition $\langle E | E \rangle = 1$.

The helical states are formed in the energy window, $|E - E_{0,\pm}| < \Delta_{\text{so}}$. We consider the states inside the energy window of the lower avoided crossing. The energy measured from the center of the energy window (dashed line in Fig. 4(a)) is, $\delta E = E - E_{0,-}$. For $\delta E > 0$, in the leading approximation (see Appendix A for detailed calculations),

$$z_{-,s'} \approx e^{-i\frac{\pi}{N}} e^{-is'(\Delta\phi + \delta k)}, \quad (29)$$

$$z_{+,s'} \approx e^{-i\frac{\pi}{N}} e^{-s'/\lambda}, \quad (30)$$

where $\lambda = 2J \sin \frac{\pi}{N} / \sqrt{\Delta_{\text{so}}^2 - \delta E^2}$ is the decay length and $\delta k = \delta E / (2J \sin \frac{\pi}{N})$ is the wave number. The former $z_{-,s'}$ corresponds to left ($s' = +$) or right ($s' = -$) going states. The latter $z_{+,s'}$ corresponds to the evanescent states with the decay length λ associated to the avoided crossing.

For $\delta E > 0$, the eigen ket is the linear combination of $|z_{-, \pm}; -\rangle$ and $|z_{+, \pm}; +\rangle$. For the state close to the center of the avoided crossing, $E \approx E_{0,-}$, it reads,

$$\begin{aligned} \psi(n) \propto e^{-i\frac{\Delta\phi}{2}} \sigma_z \left[\begin{pmatrix} 0 \\ 1 \end{pmatrix} e^{-i(\Delta\phi + \delta k)n} + a \begin{pmatrix} 1 \\ 0 \end{pmatrix} e^{i(\Delta\phi + \delta k)n} \right. \\ \left. + b \begin{pmatrix} 1 \\ i \end{pmatrix} e^{-n/\lambda} + c \begin{pmatrix} 1 \\ -i \end{pmatrix} e^{n/\lambda} \right]. \end{aligned} \quad (31)$$

The first and second terms represent the left-going \downarrow and the right-going \uparrow spins. The remaining two terms are the evanescent states that exhibit exponential behavior. They are a superposition of the \uparrow spin states in the p_x orbital (in the local coordinate). The coefficients a, b and c are determined by the three boundary conditions (Appendix B). Figures 4 (b), (c) and (d) show the local charge density and pseudo spin density of a state with the eigenenergy E' , which is the closest to $E_{0,-}$, i.e. $\langle E' | \rho_n | E' \rangle$. In each panel, the analytical result (dashed black line marked with circles) reproduces well the numerical result (solid red line). In Fig. 4 (b), an exponential increase in density is observed around each edge of the molecule. Figures 4 (c) and (d) indicate that both σ_x and σ_y are finite. However, the local spin density vanish in the total system, H_+ and H_- , because of the time reversal symmetry. We checked that the z -component of spin is nearly zero.

Note that only with the first two terms, the left-going and right-going states, it is not possible to fulfill the boundary condition Eqs. (B1) and (B2), since they have opposite spins, see discussions raised in Ref. 13 related to Ref. 14. The evanescent spins existing in the finite system can mix the two spins and necessary to fulfill the boundary condition. They are not edge state localized at the edges, since they hybridize with the left- and right-going states.

In the above discussion, we only considered H_+ . From the subsystem H_- , we obtain the same charge density with the opposite spin. Therefore, in the total system, the spin density vanishes, as expected from the time reversal symmetry of the original Hamiltonian, Eq. (4).

IV. CONCLUSION

We discuss the electron state of the two-orbital helical atomic chain with the intra-atomic spin-orbit interaction. For the infinite length and specific parameters, this model has two avoided crossings and in each energy window, there exist two helical states. We demonstrate that when the Fermi energy is in this energy window, the charge modulations concentrate at the edges. Analytically solving the wave function, we found that this happens because of the evanescent states located at the edges associated with the avoided crossing. Although the charge modulations concentrated at the edges are not spin polarized, because of the time-reversal symmetry of the Hamiltonian, we speculate that incorporating the effects of a ferromagnetic substrate, the Coulomb interaction and/or the lattice vibrations¹⁵⁻¹⁹, may have a possible impact on the enantioselectivity.

ACKNOWLEDGMENTS

This work was supported by JSPS KAKENHI Grants No. 18KK0385, No. 20H01827 and No. 20H02562.

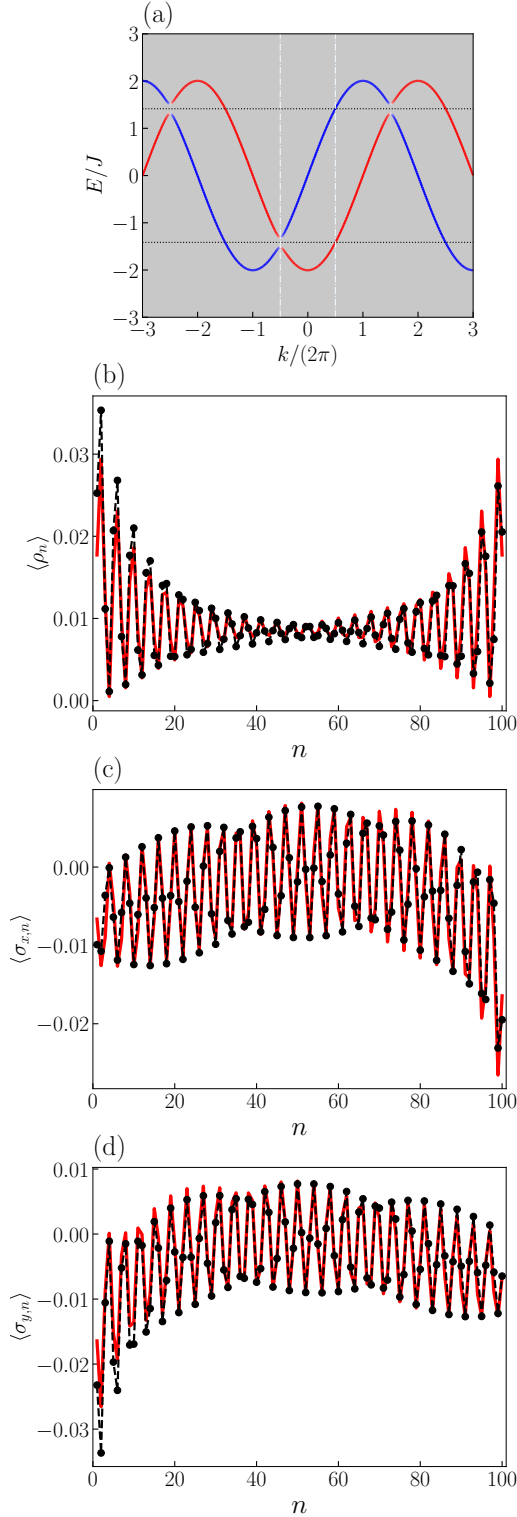


FIG. 4. (a) Band structure of H_+ . Upper and lower dashed horizontal lines indicate the center of avoided crossings $E_{0,\pm} = \pm 2J \cos \frac{\pi}{N}$. The vertical line indicates the first Brillouin zone. The local charge density (a) and spin densities (b) σ_x and (c) σ_y , of a state at $\delta E/J = 0.035$, which is close to $E_{0,-}$. In each panel, the solid red (dashed black) line represents the numerical (analytical) result. Parameters: $M = 25$, $N = 4$, $\Delta_{\text{so}}/J = 0.1$.

Appendix A: Detailed derivations

Equation (26) can be expanded up to the accuracy of δE^2 and Δ_{so}^2 as,

$$\xi_s \approx 1 + (s-1) \left(\sin^2 \frac{\pi}{N} + \frac{\delta E}{2J} \cos \frac{\pi}{N} \right) + \frac{s}{2\lambda^2}. \quad (\text{A1})$$

For $s = -$, by substituting Eq. (A1) into Eq. (25), we obtain Eq. (29) up to δE accuracy. Then by using Eq. (18), we obtain

$$E_A(z_{-,s'}) \approx s' 2J \sin \frac{\pi}{N} \sin 2\zeta. \quad (\text{A2})$$

Where $\zeta = \sqrt{\sin^2 \left(\frac{\pi}{N} \right) + \left(\frac{\delta E}{2J} \right) \cos \frac{\pi}{N}}$. Considering the conditions, $|E_A(z_{-,s'})| \gg \Delta_{\text{so}}$, Eqs. (23) and (24) become,

$$u(z_{-,s'}) \approx \sqrt{\frac{1}{2}(1-s')} = \delta_{s',-}, \quad (\text{A3})$$

$$v(z_{-,s'}) \approx \sqrt{\frac{1}{2}(1+s')} = \delta_{s',+}. \quad (\text{A4})$$

Here we used $p = 1$. Then the wave functions of left and right going states are,

$$\begin{aligned} \begin{pmatrix} \langle n; \uparrow | z_{-,s'}; + \rangle \\ \langle n; \downarrow | z_{-,s'}; + \rangle \end{pmatrix} &= z_{-,s'}^n \begin{pmatrix} v(z_{-,s'}) \\ u(z_{-,s'}) e^{i\phi_n} \end{pmatrix} \\ &\approx e^{-i\frac{\phi_n}{2} \sigma_z} e^{-is'(\phi_n + \delta kn)} \begin{pmatrix} \delta_{s',+} \\ \delta_{s',-} \end{pmatrix}, \end{aligned} \quad (\text{A5})$$

$$\begin{aligned} \begin{pmatrix} \langle n; \uparrow | z_{-,s'}; - \rangle \\ \langle n; \downarrow | z_{-,s'}; - \rangle \end{pmatrix} &= z_{+,s'}^n \begin{pmatrix} u(z_{-,s'}) \\ -v(z_{-,s'}) e^{i\phi_n} \end{pmatrix} \\ &\approx e^{-i\frac{\phi_n}{2} \sigma_z} e^{-is'(\phi_n + \delta kn)} \begin{pmatrix} \delta_{s',-} \\ -\delta_{s',+} \end{pmatrix}. \end{aligned} \quad (\text{A6})$$

Similarly for $s = +$, we obtain, Eq. (30) up to $1/\lambda$ accuracy and

$$E_A(z_{+,s'}) = -i 2J \sin \frac{\pi}{N} \sinh(s'/\lambda) \approx -is' \sqrt{\Delta_{\text{so}}^2 - \delta E^2}, \quad (\text{A7})$$

Then the wave functions of evanescent states are,

$$\begin{pmatrix} \langle n; \uparrow | z_{+,s'}; + \rangle \\ \langle n; \downarrow | z_{+,s'}; + \rangle \end{pmatrix} \approx e^{-i\frac{\phi_n}{2} \sigma_z} e^{-s'n/\lambda} \begin{pmatrix} \sqrt{\frac{1}{2} \left(1 - is' \frac{\sqrt{\Delta_{\text{so}}^2 - \delta E^2}}{|\delta E|} \right)} \\ \sqrt{\frac{1}{2} \left(1 + is' \frac{\sqrt{\Delta_{\text{so}}^2 - \delta E^2}}{|\delta E|} \right)} \end{pmatrix}, \quad (\text{A8})$$

$$\begin{pmatrix} \langle n; \uparrow | z_{+,s'}; - \rangle \\ \langle n; \downarrow | z_{+,s'}; - \rangle \end{pmatrix} \approx e^{-i\frac{\phi_n}{2} \sigma_z} e^{-s'n/\lambda} \begin{pmatrix} \sqrt{\frac{1}{2} \left(1 + is' \frac{\sqrt{\Delta_{\text{so}}^2 - \delta E^2}}{|\delta E|} \right)} \\ -\sqrt{\frac{1}{2} \left(1 - is' \frac{\sqrt{\Delta_{\text{so}}^2 - \delta E^2}}{|\delta E|} \right)} \end{pmatrix}. \quad (\text{A9})$$

Close to the center of the lower avoided crossing, $|\delta E| \ll \Delta_{so}$, they are

$$\begin{pmatrix} \langle n; \uparrow | z_{+,s'}; + \rangle \\ \langle n; \downarrow | z_{+,s'}; + \rangle \end{pmatrix} \approx e^{-i\frac{\phi_n}{2} \sigma_z} e^{-s'n/\lambda} \sqrt{\frac{\Delta_{so}}{2|\delta E|}} \begin{pmatrix} e^{-is'\pi/4} \\ e^{is'\pi/4} \end{pmatrix}, \quad (\text{A10})$$

$$\begin{pmatrix} \langle n; \uparrow | z_{+,s'}; - \rangle \\ \langle n; \downarrow | z_{+,s'}; - \rangle \end{pmatrix} \approx e^{-i\frac{\phi_n}{2} \sigma_z} e^{-s'n/\lambda} \sqrt{\frac{\Delta_{so}}{2|\delta E|}} \begin{pmatrix} e^{is'\pi/4} \\ -e^{-is'\pi/4} \end{pmatrix}. \quad (\text{A11})$$

The linear combination,

$$\begin{aligned} |E\rangle = & -|z_{-,+}; -\rangle + a|z_{-,-}; -\rangle \\ & + be^{i\pi/4} \sqrt{\frac{2|\delta E|}{\Delta_{so}}} |z_{+,+}; +\rangle + ce^{-i\pi/4} \sqrt{\frac{2|\delta E|}{\Delta_{so}}} |z_{+,-}; +\rangle, \end{aligned} \quad (\text{A12})$$

results in Eq. (31).

Appendix B: Coefficients of wave function

To determine the coefficients, we consider the following boundary condition,

$$\ell_+(0) = \ell_+(MN+1) = 0, \quad (\text{B1})$$

$$\ell_-(0) = \ell_-(MN+1) = 0, \quad (\text{B2})$$

where $\ell_{\pm}(n) = \psi_{\uparrow}(n) \pm \psi_{\downarrow}(n)$. The 3 coefficients in Eq. (31) are,

$$a = [(i-1)(i+\alpha^2)\beta + i(\alpha^2-1)\gamma + 2\alpha\beta\gamma + \beta^2(\gamma + \alpha(\alpha\gamma-2))]/R, \quad (\text{B3})$$

$$b = -\frac{\alpha(\beta+\gamma)(-\beta-i\gamma+\alpha(i+\beta\gamma))}{R}, \quad (\text{B4})$$

$$c = \frac{(\beta+\gamma)(i+\alpha(\beta-i\gamma)-\beta\gamma)}{R}. \quad (\text{B5})$$

where

$$\alpha = e^{(MN+1)/\lambda}, \quad (\text{B6})$$

$$\beta = e^{i(MN+1)\Delta\phi/2}, \quad (\text{B7})$$

$$\gamma = e^{i(MN+1)(\Delta\phi+\delta k)}, \quad (\text{B8})$$

$$R = \gamma[-1 - 2\alpha(\beta-\gamma) - i\beta(\beta + (1+i)\gamma) + \alpha^2(-1 + i\beta^2 + (1+i)\beta\gamma)]. \quad (\text{B9})$$

To obtain Fig. 4, we calculate (here, we denote ρ as σ_0)

$$\frac{\psi(n)^\dagger \sigma_i \psi(n)}{\sum_{n=1}^{MN} \psi(n)^\dagger \psi(n)} \quad (i = 0, x, y). \quad (\text{B10})$$

¹S. Mishra, A. K. Mondal, S. Pal, T. K. Das, E. Z. B. Smolinsky, G. Siligardi, and R. Naaman, "Length-dependent electron spin polarization in oligopeptides and dna," *Journal of Physical Chemistry C* **124**, 10776–10782 (2020).

²F. Evers, A. Aharony, N. Bar-Gill, O. Entin-Wohlman, P. Hedegard, O. Hod, P. Jelinek, G. Kamieniarz, M. Lemesko, K. Michaeli, V. Mujica, R. Naaman, Y. Paltiel, S. Refaely-Abramson, O. Tal, J. Thijssen, M. Thoss, J. M. van Ruitenbeck, L. Venkataraman, D. H. Waldeck, B. Yan, and L. Kronik, "Theory of chirality induced spin selectivity: Progress and challenges," *The Journal of Physical Chemistry Letters* **13**, 7 (2022).

³K. Banerjee-Ghosh, O. B. Dor, F. Tassinari, E. Capua, S. Yochelis, A. Capua, S.-H. Yang, S. S. P. Parkin, S. Sarkar, L. Kronik, L. T. Baczewski, R. Naaman, and Y. Paltiel, "Separation of enantiomers by their enantiospecific interaction with achiral magnetic substrates," *Science* **360**, 1331–1334 (2018).

⁴R. Naaman, Y. Paltiel, and D. H. Waldeck, "Chiral induced spin selectivity gives a new twist on spin-control in chemistry," *Accounts of Chemical Research* **53**, 2659–2667 (2020).

⁵B. P. Bloom, Y. Lu, T. Metzger, S. Yochelis, Y. Paltiel, C. Fontanesi, S. Mishra, F. Tassinari, R. Naaman, and D. H. Waldeck, "Asymmetric reactions induced by electron spin polarization," *Phys. Chem. Chem. Phys.* **22**, 21570–21582 (2020).

⁶A. Kumar, E. Capua, M. K. Kesharwani, J. M. L. Martin, E. Sitbon, D. H. Waldeck, and R. Naaman, "Chirality-induced spin polarization places symmetry constraints on biomolecular interactions," *Proceedings of the National Academy of Sciences* **114**, 2474–2478 (2017).

⁷J. Fransson, "Charge and spin dynamics and enantioselectivity in chiral molecules," *The Journal of Physical Chemistry Letters* **13**, 808–814 (2022).

⁸J.-i. Kishine, H. Kusunose, and H. M. Yamamoto, "On the definition of chirality and enantioselective fields," *Israel Journal of Chemistry* **62**, e202200049 (2022).

⁹H. Alpern, K. Yavilberg, T. Dvir, N. Sukenik, M. Klang, S. Yochelis, H. Cohen, E. Grosfeld, H. Steinberg, Y. Paltiel, and O. Millo, "Magnetic-related states and order parameter induced in a conventional superconductor by nonmagnetic chiral molecules," *Nano Letters* **19**, 5167–5175 (2019).

¹⁰Y. Utsumi, T. Kato, O. Entin-Wohlman, and A. Aharony, "Spin-filtering in a p -orbital helical atomic chain," *Israel Journal of Chemistry* **62**, e202200107 (2022).

¹¹Y. Utsumi, O. Entin-Wohlman, and A. Aharony, "Spin selectivity through time-reversal symmetric helical junctions," *Phys. Rev. B* **102**, 035445 (2020).

¹²S. Matityahu, Y. Utsumi, A. Aharony, O. Entin-Wohlman, and C. A. Balsero, "Spin-dependent transport through a chiral molecule in the presence of spin-orbit interaction and nonunitary effects," *Phys. Rev. B* **93**, 075407 (2016).

¹³O. Entin-Wohlman, A. Aharony, and Y. Utsumi, "Comment on "spin-orbit interaction and spin selectivity for tunneling electron transfer in dna,"" *Phys. Rev. B* **103**, 077401 (2021).

¹⁴S. Varela, I. Zambrano, B. Berche, V. Mujica, and E. Medina, "Spin-orbit interaction and spin selectivity for tunneling electron transfer in dna," *Phys. Rev. B* **101**, 241410 (2020).

¹⁵A. Kato, H. M. Yamamoto, and J.-i. Kishine, "Chirality-induced spin filtering in pseudo jahn-teller molecules," *Phys. Rev. B* **105**, 195117 (2022).

¹⁶J. Fransson, "Vibrational origin of exchange splitting and "chiral-induced spin selectivity,"" *Physical Review B* **102** (2020), 10.1103/PhysRevB.102.235416.

¹⁷D. Klein and K. Michaeli, "Giant chirality-induced spin selectivity of polarons," *Phys. Rev. B* **107**, 045404 (2023).

¹⁸C. Vittmann, R. K. Kessing, J. Lim, S. F. Huelga, and M. B. Plenio, "Interface-induced conservation of momentum leads to chiral-induced spin selectivity," *The Journal of Physical Chemistry Letters* **13**, 1791–1796 (2022).

¹⁹C. Vittmann, J. Lim, D. Tamascelli, S. F. Huelga, and M. B. Plenio, "Spin-dependent momentum conservation of electron-phonon scattering in chirality-induced spin selectivity," *The Journal of Physical Chemistry Letters* **14**, 340–346 (2023).